Optical Ramsey fringes with traveling waves

Ch. J. Bordé, Ch. Salomon, S. Avrillier, A. Van Lerberghe, and Ch. Bréant
Laboratoire de Physique des Lasers (Laboratoire No. 282 associé au Centre National de la Recherche Scientifique), Université de Paris—Nord, F-93430 Villetaneuse, France

D. Bassi
Istituto per la Ricerca Scientifica e Technologica, I-38050 Povo, Italy

G. Scoles
Department of Chemistry, University of Waterloo, Waterloo, Ontario, Canada N2L 3G1
(Received 12 January 1984)

We present a new interaction geometry for optical Ramsey fringes comprised of four traveling waves instead of the three usual standing waves. First, we demonstrate experimentally that the new method leads to an improved contrast, using the optothermal detection of the vibrational excitation of SF_6 in a supersonic beam illuminated by a waveguide CO_2 laser. Second, we give a simple theoretical description of the method, using evolution matrices of spinors and pseudospin-vector representations of these spinors. Finally, we introduce strong-field density-matrix diagrams to discuss the differences between the various interaction geometries as well as between the Ramsey fringes and the usual stimulated photon echoes.

I. INTRODUCTION

As soon as the finite transit time was identified as the basic limitation to ultra-high resolution in saturation spectroscopy, it was suggested[1] to associate sub-Doppler techniques with the method of spatially separated fields introduced by Ramsey in the microwave domain around 1950.[2] The first realistic proposals came from Novosibirsk for saturation spectroscopy[3] and for Doppler-free two-photon spectroscopy. [4] In saturation spectroscopy the Russian method uses three equidistant standing waves and the early experimental demonstrations have used this interaction geometry.[5–9] In an independent theoretical study, one of us showed that fringes resulted from successive interactions with four traveling waves[10,11] and it became clear that one could also obtain fringes with four spatially separated traveling waves with a number of advantages over the three standing-waves method. In the first part of this paper, we present an experimental comparison between the standing waves and the traveling-waves interaction geometries, using an optothermal detection technique[12] to monitor the vibrational excitation in a supersonic beam of SF_6. In the second part of the paper we give a detailed description of the new method in terms of spinors and of pseudospin trajectory. The difference with usual stimulated photon echoes[13] is emphasized. A new graphical representation, the strong-field density-matrix diagrams, is introduced to discuss further this difference and to provide a direct comparison with the standing-waves case as well as with the mixed case introduced by Shimoda and co-workers.[14]

We shall see that with four traveling waves the physical origin of optical Ramsey fringes becomes especially simple to understand. Let us recall, that in the usual Ramsey interaction scheme, the induced polarization precesses freely between two field zones. As a result of the phase comparison between this polarization and the field in the second zone, final populations oscillate as a function of detuning and time of flight between the two field zones. Unfortunately, in the optical domain, the distribution of first-order Doppler shifts averages out the fringes. To solve this problem, our interaction geometry is such that the previous usual Ramsey operation is simply repeated with a second pair of laser beams traveling in a direction opposite to that of the first pair. The populations which oscillate as a function of laser detuning and velocity after interaction with the first pair, give rise to two distinct contributions through interaction with the second pair. One for which the Doppler dephasing is canceled and for which only the oscillatory behavior with detuning subsists; this is the Ramsey fringes signal. One which loses its oscillatory behavior with detuning but for which the Doppler dephasing is doubled; this is the backward stimulated photon echo which averages to zero by velocity integration.

Ideally, a succession of $\pi/2$ pulses then results clearly in maximum signal for the fringes. As we shall see in detail the situation is far more complicated with standing waves for which the simultaneous interaction with oppositely traveling waves reduces the fringe contrast.

II. EXPERIMENTAL RESULTS

In order to investigate optical Ramsey fringes experimentally, we have used a supersonic SF_6 beam illuminated either by a triple standing wave or by four traveling waves from a waveguide CO_2 laser. The schematic diagram of the molecular beam apparatus can be found in Ref. 15. The supersonic beam is obtained by adiabatic expansion of 7 vol% SF_6—He mixture through a 50 μm nozzle fol-

lowed by a 0.5-mm cross-sectional diameter skimmer located about 1 cm downstream from the nozzle. The supersonic beam then enters the interaction chamber where the background pressure is of the order of 3×10^{-6} Torr the presence of beam. The flow velocity of the SF_6 molecules estimated from the observed Ramsey fringe period is 940 m/s, in good agreement with time-of-flight measurements in similar conditions.[16] In the first experiment the beam crossed the three standing waves generated from a single Gaussian beam (beam waist radius 6 mm) by a set of three slits 1 mm wide and 5 mm apart from each other and by a retroreflector [see Fig. 1(a)].

Before the introduction of this optical setup inside the interaction chamber, the laser beam waist had been carefully positioned on the molecular beam by optimizing the Rabi oscillations contrast as described in Refs. 15 and 17. In a second series of experiments two slits only were illuminated and the two transmitted waves were reflected by the triedron with a spatial offset equal to 15 mm in order to generate two pairs of traveling waves [see Fig. 1(b)].

The three components A_1,F_1,E of the ν_3 band $P(4)$ manifold can be reached with a waveguide CO_2 laser oscillating on the $P(16)$ CO_2 line at 10.55 μm. This laser was slaved by a frequency offset—locking technique to a conventional low-pressure CO_2 laser which was itself locked to the $Q(43)$ F_1^8 saturation resonance of SF_6. This technique provides both a very good short-term spectral width ($\simeq$10 Hz) and the possibility to scan the frequency with an auxiliary RF synthesizer.[18]

After their interaction with the three or four light beams the molecules hit the liquid He-cooled surface of a silicon bolometer (1×5 mm^2) where they leave their internal energy. Since the laser beam is chopped, only the modulated rovibrational contribution of this internal energy is detected as a signal by standard lock-in techniques.[12] The bolometer is placed 48 cm away from the skimmer. Its electrical characteristics at 4.2 K are a 4×10^4 V/W responsivity and a NEP (noise equivalent power) of 8×10^{-13} W/$\sqrt{\text{Hz}}$ at 30 Hz. However, in working conditions with a molecular beam, this NEP was observed to increase by one order of magnitude. Nevertheless as illustrated in Figs. 1(a) and 1(b) beautiful fringes have been obtained with both interaction geometries. These two figures also illustrate the large difference in fringe contrast (factor 2 to 3) which is obtained between these two cases. This difference is most easily understood in a theoretical approach, using transformation matrices, which we outline below.

III. THEORETICAL FRAMEWORK

Any realistic theory of optical Ramsey fringes should take into account transit effects, relaxation, first and second-order Doppler broadening and shifts as well as the recoil effect. All these effects are built in the following approach and no restrictive assumption is made concerning their respective importance. The individual atomic response is calculated as a function of molecular velocity and then averaged over initial formation conditions (velocity distribution or more generally phase-space distribution in a molecular beam).

We consider a two-level system interacting with a number of traveling waves which all have the same frequency but which may propagate in two opposite directions ($+$ or $-$). In the molecular frame of reference defined by $\vec{v}=\vec{p}_0/M\gamma$ for molecules formed in the lower level a with a momentum $\vec{p}_0$ [$\gamma=(1-v^2/c^2)^{-1/2}$] we shall write the electric fields as

$$\vec{\mathscr{E}}(\vec{r},t)=\mathrm{Re}\,\hat{e}^{\pm}E^{\pm}U^{\pm}[v_x(t-t_1)] \times\exp[i(\gamma\omega t\mp kv_z t\mp kz+\varphi^{\pm})]\,, \tag{1}$$

where $\hat{e}$, E, U, and φ represent, respectively, the polarization vector, the amplitude, the transverse dependence and the phase of each wave. The fields are propagating along the $\hat{z}$ axis and for the sake of simplicity, in this paper, we shall ignore the y direction (molecular flow along the $\hat{x}$ axis) and assume that the function U is real and symmetric about the time t_1. These fields couple together a large number of energy-momentum states as illustrated in Fig. 2.

In the $|\vec{r}\rangle$ representation, the wave-function components for each state $\alpha=a,b$ can be written as a discrete sum (Fourier series) where each component $\alpha_m(\vec{r},t)$ corresponds to an energy-momentum state[19]

$$\langle\alpha\,|\,\psi(\vec{r},t)\rangle=\sum_m\langle\alpha_m\,|\,\psi(\vec{r},t)\rangle=\sum_m\alpha_m(\vec{r},t)\,, \tag{2}$$

where

$$\langle\alpha_m\,|\,\psi(\vec{r},t)\rangle=\int_{m\hbar\vec{k}}d^3p\langle\vec{r}\,|\,\vec{p}\rangle\langle\vec{p}\,|\,\langle\alpha\,|\,\psi(t)\rangle$$

is an $\vec{r}$ wave packet centered about each momentum $m\hbar\vec{k}$ (m is an integer corresponding to the net number of momentum quanta exchanged with the field from $\vec{p}_0$). The molecular system can be described either by the spinor

$$\begin{bmatrix}\langle b\,|\,\psi(\vec{r},t)\rangle\\ \langle a\,|\,\psi(\vec{r},t)\rangle\end{bmatrix}=\begin{bmatrix}\sum_m b_m(\vec{r},t)\\ \sum_m a_m(\vec{r},t)\end{bmatrix}$$

or by a vector with an infinite number of components written as

$$\begin{bmatrix}\vdots\\ a_{m+2}\\ b_{m+1}\\ a_m\\ b_{m-1}\\ \vdots\end{bmatrix}.$$

The first description which was used in Refs. 20 and 21 is easier to deal with (2×2 tranformation matrices) but is not as general as the second; for example, owing to the recoil effect a different energy

$$E_\alpha+m^2(\hbar k)^2/2M=E_\alpha+m^2\hbar\delta$$

is associated with each α_m and this correction is obviously easier to introduce in the second approach; the first approach requires successive rotating frame transformation which can be avoided in the second. In this paper we therefore emphasize this second formalism.

The Schrödinger equation can be written in matrix form

$$\frac{\partial}{\partial t}\begin{bmatrix}\vdots\\ a_{m+2}\\ b_{m+1}\\ a_m\\ b_{m-1}\\ \vdots\end{bmatrix}=\begin{bmatrix}\cdots & -i\frac{E_a}{\hbar}-i(m+2)^2\delta-\frac{\gamma_a}{2} & 0 & 0 & 0 & \cdots\\ \cdots & 0 & -i\frac{E_b}{\hbar}-i(m+1)^2\delta-\frac{\gamma_b}{2} & 0 & 0 & \cdots\\ \cdots & 0 & 0 & -i\frac{E_a}{\hbar}-im^2\delta-\frac{\gamma_a}{2} & 0 & \cdots\\ \cdots & 0 & 0 & 0 & -i\frac{E_b}{\hbar}-i(m-1)^2\delta-\frac{\gamma_b}{2} & \cdots\end{bmatrix}$$

$$+i\begin{bmatrix}\cdots & 0 & \Omega_{ba}^{-}U^{-}e^{i(\gamma\omega t+kv_zt+kz+\varphi^-)} & 0 & 0 & \cdots\\ \cdots & \Omega_{ba}^{-}U^{-}e^{-i(\gamma\omega t+kz+kv_zt+\varphi^-)} & 0 & \Omega_{ba}^{+}U^{+}e^{-i(\gamma\omega t-kz-kv_zt+\varphi^+)} & 0 & \cdots\\ \cdots & 0 & \Omega_{ba}^{+}U^{+}e^{+i(\gamma\omega t-kz-kv_zt+\varphi^+)} & 0 & \Omega_{ba}^{-}U^{-}e^{i(\gamma\omega t+kz+kv_zt+\varphi^-)} & \cdots\\ \cdots & 0 & 0 & \Omega_{ba}^{-}U^{-}e^{-i(\gamma\omega t+kz+kv_zt+\varphi^-)} & 0 & \cdots\end{bmatrix}\begin{bmatrix}\vdots\\ a_{m+2}\\ b_{m+1}\\ a_m\\ b_{m-1}\\ \vdots\end{bmatrix} \tag{3}$$

where we have made the rotating-wave approximation, where $\delta=\hbar k^2/2M$, where $\Omega_{ba}^{\pm}=\langle b\mid\vec{\mu}\cdot\hat{e}^{\pm *}\mid a\rangle E^{\pm}/2\hbar$ are Rabi pulsations, and where γ_a and γ_b are relaxation constants associated with levels a and b. The following unitary transformation can be used to obtain a Hamiltonian matrix independent of space and time (apart from the slow time dependence of U):

$$\begin{bmatrix}\vdots\\ \tilde{a}_{m+2}\\ \tilde{b}_{m+1}\\ \tilde{a}_m\\ \tilde{b}_{m-1}\\ \vdots\end{bmatrix}=\exp\left[\frac{i}{2}(E_b+E_a)t/\hbar\right]\begin{bmatrix}\cdots & e^{i/2[-\gamma\omega t-2(m+2)k(z+v_zt)]} & 0 & 0 & 0 & \cdots\\ \cdots & 0 & e^{i/2[\gamma\omega t-2(m+1)k(z+v_zt)]} & 0 & 0 & \cdots\\ \cdots & 0 & 0 & e^{i/2[-\gamma\omega t-2mk(z+v_zt)]} & 0 & \cdots\\ \cdots & 0 & 0 & 0 & e^{i/2[\gamma\omega t-2(m-1)k(z+v_zt)]} & \cdots\end{bmatrix}\begin{bmatrix}\vdots\\ a_{m+2}\\ b_{m+1}\\ a_m\\ b_{m-1}\\ \vdots\end{bmatrix}, \tag{4}$$

The evolution equation for the transformed vector is

$$\frac{\partial}{\partial t}\begin{vmatrix}\vdots\\ \tilde{a}_{m+2}\\ \tilde{b}_{m+1}\\ \tilde{a}_m\\ \tilde{b}_{m-1}\\ \vdots\end{vmatrix}=\left[\begin{bmatrix}\cdots & -\frac{i}{2}(\gamma\omega-\omega_0)-i(m+2)^2\delta-\frac{\gamma_a}{2}-i(m+2)kv_z & 0 & 0 & \cdots\\ \cdots & 0 & \frac{i}{2}(\gamma\omega-\omega_0)-i(m+1)^2\delta-\frac{\gamma_b}{2}-i(m+1)kv_z & 0 & \cdots\\ \cdots & 0 & 0 & -\frac{i}{2}(\gamma\omega-\omega_0)-im^2\delta-\frac{\gamma_a}{2}-imkv_z & \cdots\\ \cdots & 0 & 0 & 0 & \frac{i}{2}(\gamma\omega-\omega_0)-i(m-1)^2\delta-\frac{\gamma_b}{2}-i(m-1)kv_z\end{bmatrix}\right.$$

$$\left.+i\begin{bmatrix}\cdots & 0 & \Omega_{ba}^{-}U^{-}e^{i\varphi^{-}} & 0 & 0 & \cdots\\ \cdots & \Omega_{ba}^{-}U^{-}e^{-i\varphi^{-}} & 0 & \Omega_{ba}^{+}U^{+}e^{-i\varphi^{+}} & 0 & \cdots\\ \cdots & 0 & \Omega_{ba}^{+}U^{+}e^{+i\varphi^{+}} & 0 & \Omega_{ba}^{-}U^{-}e^{i\varphi^{-}} & \cdots\\ \cdots & 0 & 0 & \Omega_{ba}^{-}U^{-}e^{-i\varphi^{-}} & 0 & \cdots\end{bmatrix}\right]\begin{vmatrix}\vdots\\ \tilde{a}_{m+2}\\ \tilde{b}_{m+1}\\ \tilde{a}_m\\ \tilde{b}_{m-1}\\ \vdots\end{vmatrix}, \tag{5}$$

where $\omega_0=(E_b-E_a)/\hbar$.

IV. CASE OF SPATIALLY SEPARATED TRAVELING WAVES

In the case of interactions with purely traveling waves, the above Hamiltonian matrix can be broken into 2×2 sub-blocks and we may consider independently the evolution of spinors such that

$$\begin{bmatrix}\tilde{b}_{m\pm1}\\ \tilde{a}_m\end{bmatrix}$$

for which the Schrödinger equation reduces to

$$\frac{\partial}{\partial t}\begin{bmatrix}\tilde{b}_{m\pm1}\\ \tilde{a}_m\end{bmatrix}=\frac{i}{2}\left[\vec{\Omega}\cdot\vec{\sigma}+\Omega_0\sigma_0\right]\begin{bmatrix}\tilde{b}_{m\pm1}\\ \tilde{a}_m\end{bmatrix}, \tag{6}$$

where the choice of sign is imposed by the direction of the wave and where we have introduced the Pauli matrices σ_0,

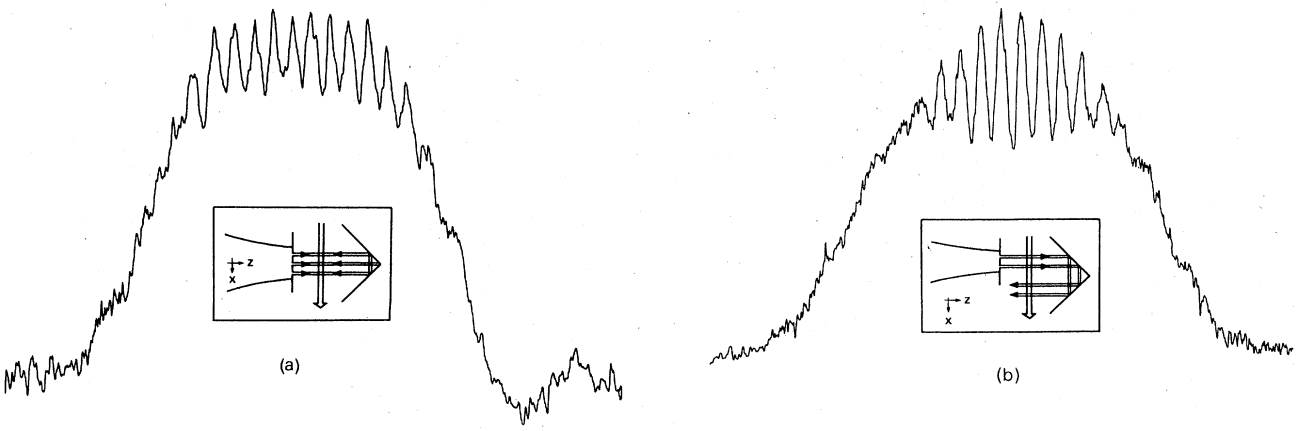

FIG. 1. (a) Ramsey pattern obtained for the $P(4)$ F_1 SF_6 line with three standing waves (interaction geometry illustrated by the inset). The horizontal scale is linear in frequency and one fringe period corresponds to 94 kHz. The laser power was adjusted for optimum fringe contrast. The signal was recorded in a single one-minute sweep with a 0.1 s time constant and a 30 Hz modulation frequency of the laser amplitude. (b) Same as (a) with four traveling waves.

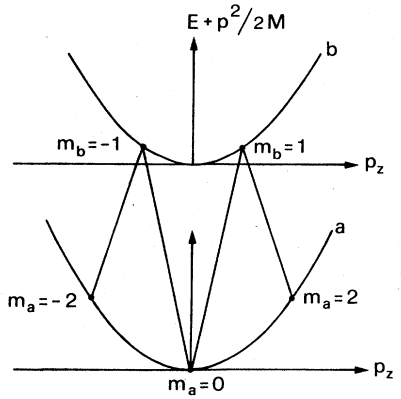

FIG. 2. Energy-momentum states of a two-level system coupled by counter-propagating laser beams.

$\vec{\sigma}$ and the effective field

$$\vec{\Omega}\begin{cases}\Omega_1=2\Omega_{ba}^{\pm}U^{\pm}\cos\varphi^{\pm}, \\ \Omega_2=2\Omega_{ba}^{\pm}U^{\pm}\sin\varphi^{\pm}, \\ \Omega_3=\Delta\mp kv_z-[(m\pm1)^2-m^2]\delta+i(\gamma_b-\gamma_a)/2, \end{cases} \tag{7}$$

$$\Omega_0=-[(m\pm1)^2+m^2]\delta-(2m\pm1)kv_z+i\gamma_{ba}, \tag{8}$$

and where $\Delta=\gamma\omega-\omega_0$ and $\gamma_{ba}=(\gamma_b+\gamma_a)/2$.

If the field amplitude is constant in each field zone, $U^{\pm}\equiv1$ and Eq. (6) is easily integrated from time t_0 to time t

$$\begin{bmatrix}\tilde{b}_{m\pm1}(t)\\ \tilde{a}_m(t)\end{bmatrix}=\exp\left[\frac{i}{2}\Omega_0\sigma_0(t-t_0)\right]\exp\left[\frac{i}{2}\vec{\Omega}\cdot\vec{\sigma}(t-t_0)\right]\begin{bmatrix}\tilde{b}_{m\pm1}(t_0)\\ \tilde{a}_m(t_0)\end{bmatrix}, \tag{9}$$

where the operator $\exp[i/2\vec{\Omega}\cdot\vec{\sigma}(t-t_0)]$ is easily expressed as [parametrization formula of the group $SL(2C)$]

$$\exp\left[\frac{i}{2}\vec{\Omega}\cdot\vec{\sigma}(t-t_0)\right]=\sigma_0\cos\left[\frac{\Omega(t-t_0)}{2}\right]+i\hat{n}\cdot\vec{\sigma}\sin\left[\frac{\Omega(t-t_0)}{2}\right]=\begin{bmatrix}A & Be^{-i\varphi^{\pm}}\\ Ce^{i\varphi^{\pm}} & D\end{bmatrix} \tag{10}$$

with

$$\hat{n}=\vec{\Omega}/\Omega \tag{11}$$

and

$$\Omega^2=\vec{\Omega}^2=\Omega_3^2+4\Omega_{ba}^2 \tag{12}$$

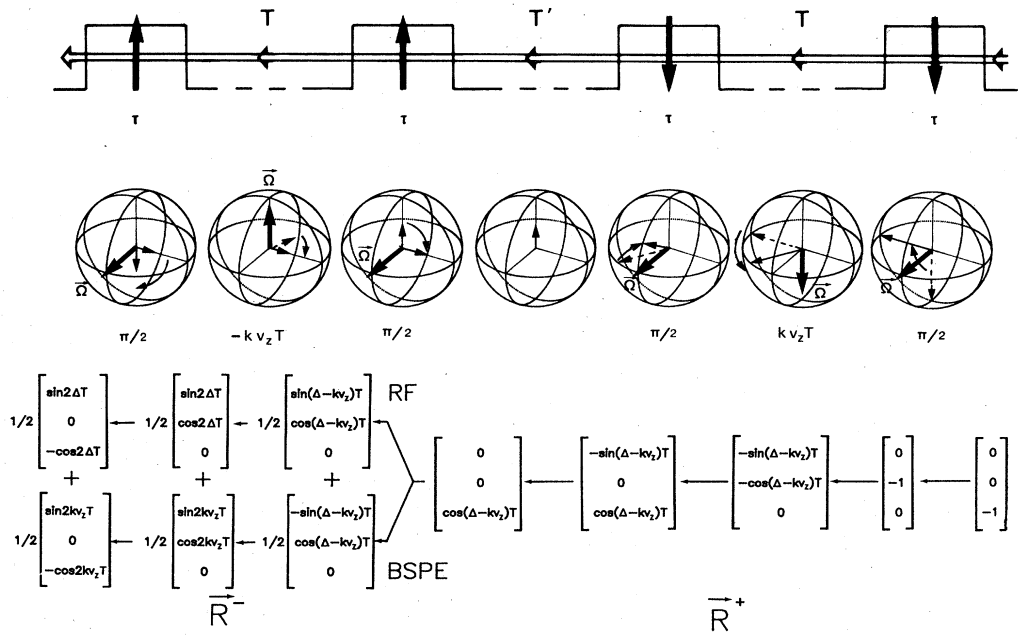

FIG. 3. Principle and illustration of Ramsey fringes (RF) with four traveling waves. At each step we give the three components of the relevant pseudospin $\vec{R}^{\pm}$. The backward stimulated photon echo (BSPE) would correspond to a vector $\vec{R}_{adv}^{-}$ (not represented) which doubles its Doppler dephasing.

and where

$$A=\cos\left[\frac{\Omega(t-t_0)}{2}\right]+i\frac{\Omega_3}{\Omega}\sin\left[\frac{\Omega(t-t_0)}{2}\right],\quad D=\cos\left[\frac{\Omega(t-t_0)}{2}\right]-i\frac{\Omega_3}{\Omega}\sin\left[\frac{\Omega(t-t_0)}{2}\right],$$
$$B=C=2i\frac{\Omega ba}{\Omega}\sin\left[\frac{\Omega(t-t_0)}{2}\right]. \tag{13}$$

We recover a 2×2 formalism which leads to very simple line-shape calculations by straightforward multiplication of 2×2 matrices corresponding to successive interaction or field-free zones. Let us now illustrate this with the case of the four traveling waves represented in Fig. 3.

In the first phase the interaction with the first two $(+)$ traveling waves gives after the central dark zone

$$\begin{bmatrix}\tilde{b}_1\\ \tilde{a}_0\end{bmatrix}=\exp\left[\frac{i}{2}\Omega_0(T'+T+2\tau)\right]\begin{bmatrix}e^{i\Omega_3T'/2} & 0\\ 0 & e^{-i\Omega_3T'/2}\end{bmatrix}\begin{bmatrix}A_2 & B_2e^{-i\varphi_2^+}\\ C_2e^{i\varphi_2^+} & D_2\end{bmatrix}\begin{bmatrix}e^{i\Omega_3T/2} & 0\\ 0 & e^{-i\Omega_3T/2}\end{bmatrix}\begin{bmatrix}A_1 & B_1e^{-i\varphi_1^+}\\ C_1e^{i\varphi_1^+} & D_1\end{bmatrix}\begin{bmatrix}0\\ 1\end{bmatrix}, \tag{14}$$

where $\Omega_3=\Delta-kv_z-\delta+i(\gamma_b-\gamma_a)/2$, $\Omega_0=-\delta-kv_z+i\gamma_{ba}$ [see (7) and (8) with $m=0$]. Let us observe that a calculation of $\tilde{b}_1\tilde{b}_1^*$ from this formula gives a generalization of Ramsey's formula including relaxation, first- and second-order Doppler effect as well as the recoil.[21]

In a second phase, in which the interaction takes place with two $(-)$ field zones, we can independently describe the evolution of the spinors

$$\begin{bmatrix}\tilde{b}_1\\ \tilde{a}_2\end{bmatrix}$$

and

$$\begin{bmatrix}\tilde{b}_{-1}\\ \tilde{a}_0\end{bmatrix}$$

from

$$\begin{bmatrix}\tilde{b}_1\\ 0\end{bmatrix}\text{and}\begin{bmatrix}0\\ \tilde{a}_0\end{bmatrix}.$$

The corresponding matrices are

$$\exp\left[\frac{i}{2}\Omega_0(T+2\tau)\right]\begin{bmatrix}A_4 & B_4e^{-i\varphi_4^-}\\ C_4e^{i\varphi_4^-} & D_4\end{bmatrix}\begin{bmatrix}e^{i\Omega_3T/2} & 0\\ 0 & e^{-i\Omega_3T/2}\end{bmatrix}\begin{bmatrix}A_3 & B_3e^{-i\varphi_3^-}\\ C_3e^{i\varphi_3^-} & D_3\end{bmatrix}, \tag{15}$$

where

$$\Omega_3=\Delta+kv_z-\delta+i(\gamma_b-\gamma_a)/2,\quad \Omega_0=-\delta+kv_z+i\gamma_{ba}$$

for

$$\begin{bmatrix}\tilde{b}_{-1}\\ \tilde{a}_0\end{bmatrix}$$

and

$$\Omega_3=\Delta+kv_z+3\delta+i(\gamma_b-\gamma_a)/2,\quad \Omega_0=-5\delta-3kv_z+i\gamma_{ba}$$

for

$$\begin{bmatrix}\tilde{b}_1\\ \tilde{a}_2\end{bmatrix}.$$

Combining the two sets of matrices we find

$$\tilde{b}_{-1}\tilde{b}^*_{-1}=e^{-2\gamma_{ba}(T+2\tau)}e^{-\gamma_a T'}\{|B_1C_2B_3A_4|^2e^{-(\gamma_b-\gamma_a)T}+|B_1C_2D_3B_4|^2+|D_1D_2B_3A_4|^2+|D_1D_2D_3B_4|^2e^{(\gamma_b-\gamma_a)T}$$
$$+[B_1C_2B_3A_4(D_1D_2D_3B_4)^*e^{2i(\Delta-\delta)T}e^{i(\varphi_4^--\varphi_3^-+\varphi_2^+-\varphi_1^+)}+\text{c.c.}]$$
$$+O(e^{\pm ikv_zT}\text{ or to }e^{\pm 2ikv_zT})\}\,, \tag{16}$$

where the oscillating term $\exp[2i(\Delta-\delta)T]$ corresponds to the fringe pattern up shifted by the recoil shift δ, and

$$\tilde{b}_1\tilde{b}^*_1=e^{-2\gamma_{ba}(T+2\tau)}e^{-\gamma_b T'}\{|B_1A_2A_3A_4|^2e^{-(\gamma_b-\gamma_a)T}+|B_1A_2C_3B_4|^2+|D_1B_2A_3A_4|^2+|D_1B_2C_3B_4|^2e^{(\gamma_b-\gamma_a)T}$$
$$+[B_1A_2A_3A_4(D_1B_2C_3B_4)^*e^{2i(\Delta+\delta)T}e^{i(\varphi_4^--\varphi_3^-+\varphi_2^+-\varphi_1^+)}+\text{c.c.}]+O(e^{\pm ikv_zT},e^{\pm 2ikv_zT})\}\,, \tag{17}$$

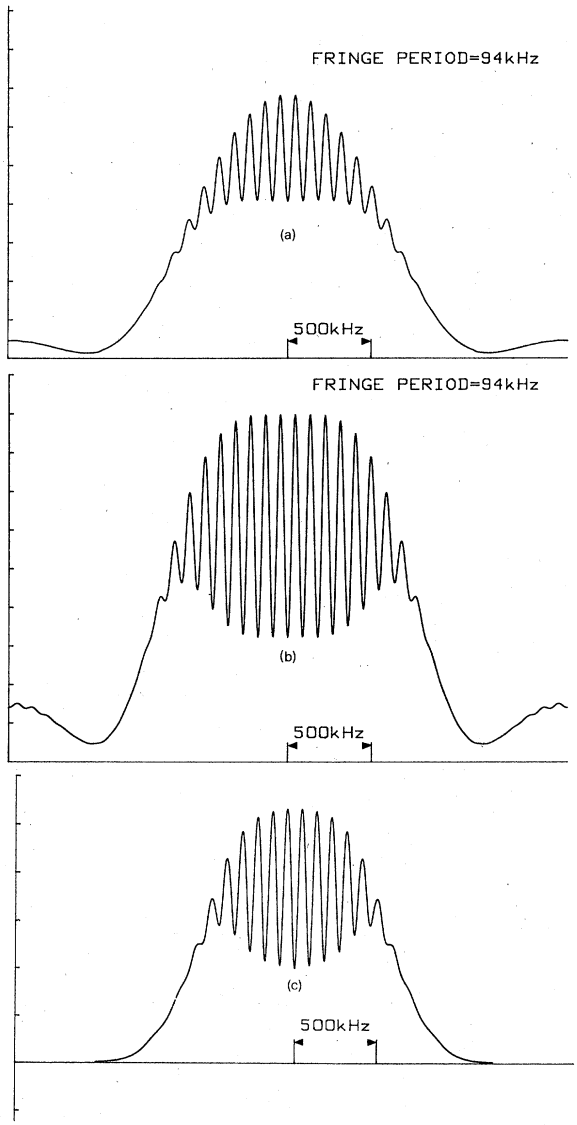

FIG. 4. Theoretical fringe patterns: (a) and (b) calculated from formulas (16) and (17) (without recoil and relaxation) with $T/\tau=5.25$ and $\Omega_1\tau=0.988$ for (a), $\Omega_1\tau=1.8$ for (b); (c) is calculated numerically for Gaussian laser profiles with a beam waist radius $w_0=0.5$ mm separated by 5 mm.

where the oscillating term $\exp 2i(\Delta+\delta)T$ corresponds to the fringe pattern down shifted by the recoil shift δ.

The signal is obtained by integration on v_z of the previous expressions. If the Doppler width is large compared to the fringe width, integrals of terms proportional to $e^{\pm ikv_zT}$ or $e^{\pm 2ikv_zT}$ are negligible; the v_z integrals of the terms in factor of $e^{2i(\Delta\pm\delta)T}$ give the fringe envelope and those of the remaining terms give the background broadened by the Doppler effect and by finite transit time. Figures 4(a) and 4(b) are typical graphs of the signal calculated from formulas (16) and (17) and numerically integrated over a flat velocity (v_z) distribution in the ideal case of four equal square pulses corresponding to $2\Omega_{ba}\tau=0.988$, for Fig. 4(a) and to the optimum value 1.8 for Fig. 4(b). (This optimum value is slightly higher than $\pi/2$ owing to the v_z dependence of Ω through Ω_3.) In this last case the fringe contrast is close to $\frac{2}{3}$. A contrast of only 40% could be reached in the actual experiment [see Fig. 1(b)] for which the signal shape is better represented by Fig. 4(a). This can be explained by a number of practical reasons: distribution of Clebsch-Gordan coefficients; y distribution of the field, hyperfine structure of the lines, wave-front imperfections, ... Also to obtain the actual signal one should perform a final integration on the narrow (13%) distribution of velocity moduli which will reduce the size of side fringes.

The signal width has contributions from transit broadening and from Doppler broadening associated with the v_z distribution of molecules impinging on the bolometer. The corresponding parameters $(\tau,\Delta v_z)$ are not very well defined in our experiment (because of light diffraction from the slits and of a lack of precise knowledge of the effective v_z distribution in the beam) and are coupled in a fit. To reproduce the signal background we have adjusted the time τ to an effective value $\frac{4}{5}$ of the value deduced from the slit width. Finally the overall shape of the signal is slightly better represented by a numerical calculation with Gaussian laser profiles as illustrated by Fig. 4(c) for the optimum value $2\Omega_{ba}w_0/v_x=1$.

V. PSEUDOSPIN REPRESENTATION

To understand in detail the origin of the fringes and their size, it is possible to follow the evolution of pseudospin vectors as illustrated in Fig. 3 in the ideal case of $\pi/2$

pulses at resonance and in the absence of relaxation.

A four-vector R can be associated to any two-component spinor

$$\begin{bmatrix} b \\ a \end{bmatrix}$$

by the formulas

$$\begin{aligned} R^1 &= ba^* + ab^* , \\ R^2 &= iba^* - ib^* a , \\ R^3 &= bb^* - aa^* , \\ R^0 &= bb^* + aa^* . \end{aligned} \tag{18}$$

If the spinor satisfies an equation as (6) the four vector satisfies[21]

$$\frac{\partial R^j}{\partial t} = -\gamma_{ba} R^j - \frac{i}{2}[\vec{\Omega}\cdot(\vec{J} - i\vec{K}) + \vec{\Omega}^*\cdot(\vec{J} + i\vec{K})]R^j , \tag{19}$$

where $\vec{J}$ and $\vec{K}$ are the generators of the Lorentz group [for the solution of (19) see Ref. 21].

In the absence of relaxation this equation reduces to the familiar gyroscopic motion equation for the pseudospin vector $\vec{R}$,[22,23]

$$\frac{\partial \vec{R}}{\partial t} = -i\Omega(\hat{n}\cdot\vec{J})\vec{R} = \vec{R}\times\vec{\Omega} , \tag{20}$$

the solution of which is easily written using the parametrization formula of the rotation group

$$\exp(-i\hat{n}\cdot\vec{J}\Theta) = I - i(\hat{n}\cdot\vec{J})\sin\Theta - (\hat{n}\cdot\vec{J})^2(1-\cos\Theta) , \tag{21}$$

where I is the unity matrix and where $\Theta = \Omega(t - t_0)$.

It is clear that calculations are easier to perform with the 2×2 matrices than with 3×3 matrices. The only advantage of $\vec{R}$ is to provide a convenient geometrical representation of transient phenomena. The difficulty which arises when one deals with optical fields having opposite directions is that $\vec{R}$ has many Fourier harmonics of the space variable z. In general this complicated spatial dependence of $\vec{R}$ deprives this geometrical model from any utility. However in the case of purely traveling waves we have seen that we could consider space-independent spinors such as

$$\begin{bmatrix} \tilde{b}_{m\pm 1} \\ \tilde{a}_m \end{bmatrix} .$$

To each of these we can associate a vector $\vec{R}_m^{\pm}$ by

$$\begin{aligned} \vec{R}_m^{\pm} = &((\tilde{a}_m \tilde{b}^*_{m\pm 1} + \text{c.c.}), (i\tilde{b}_{m\pm 1}\tilde{a}^*_m + \text{c.c.}) , \\ &(\tilde{b}_{m\pm 1}\tilde{b}^*_{m\pm 1} - \tilde{a}_m \tilde{a}^*_m)) , \end{aligned} \tag{22}$$

where the $\pm$ sign corresponds obviously to the $(+)$ and $(-)$ directions of propagation of the laser fields and where each of the $\vec{R}_m^{\pm}$ vectors satisfies an equation such as (20).

If the recoil shift is neglected we may also use the two vectors

$$\vec{R}^{\pm} = \sum_m \vec{R}_m^{\pm} \tag{23}$$

which share the same vertical component.

As an example we have represented in Fig. 3 the trajectories for $\vec{R}^+$ and $\vec{R}^-$ in the process of Ramsey fringes with four traveling waves. In the first half only $\vec{R}^+$ is coupled to the field, $\vec{R}^-$ has no horizontal component and reduces to the vertical component of $\vec{R}^+$. In the second half, only the vector $\vec{R}^-$ is coupled to the field and is represented (the horizontal components of $\vec{R}^+$ evolve freely and independently and are not represented). For the sake of simplicity we have assumed optimum pulses at resonance in each of the four field regions. The recoil shift and the relaxation have been ignored. In the first phase $\vec{R}^+$ undergoes the following sequence of events: $\pi/2$ pulse, free precession corresponding to the Doppler dephasing kv_zT, and $\pi/2$ pulse. The modulated vertical component of $\vec{R}^+$ serves as the initial condition for $\vec{R}^-$ in the next phase. After a first $\pi/2$ pulse the amplitude-modulated vector $\vec{R}^-$ is decomposed into two vectors of equal constant amplitude and opposite modulated (advanced and retarded) phases, $\vec{R}^- = \vec{R}^-_{\text{ret}} + \vec{R}^-_{\text{adv}}$. After a new free precession in a dark zone, one of these vectors cancels its Doppler phase (Ramsey fringes) whereas the other doubles it before the final $\pi/2$ pulse (stimulated backward photon echo) and only the first of these vectors is represented on the figure. This sequence of events is completely different from the usual photon echo in which:

(i) The dephasing process does not reverse as here between the first and second dark periods.

(ii) The effect of the middle interaction is a π pulse which results in a symmetry about the $(\hat{1},\hat{3})$ plane essentially different from what happens here since $\vec{R}^+$, before the central fields, and $\vec{R}^-$, after them, are collinear.

VI. STRONG-FIELD DENSITY MATRIX DIAGRAMS

A more general graphical representation of coherent processes, applicable to standing waves as well, could be a strong-field generalization of density-matrix diagrams.[11,19] Vertices of interaction with the various fields are separated by field-free regions where the free propagators are known. With the representation (4) the free propagator corresponding to a time interval T is

$$\exp\{[i(\gamma\omega - \omega_0) - i(m_b^2 - m_a^2) - i(m_b - m_a)kv_z - \gamma_{ba}]T\} \tag{24}$$

for

$$\langle m_b \,|\, \tilde{\rho}_{ba} \,|\, m_a \rangle = \tilde{b}_{m_b}\tilde{a}^*_{m_a}$$

and

$$\exp[-i(m^2 - m'^2)\delta - i(m - m')kv_z - \gamma_a]T \tag{25}$$

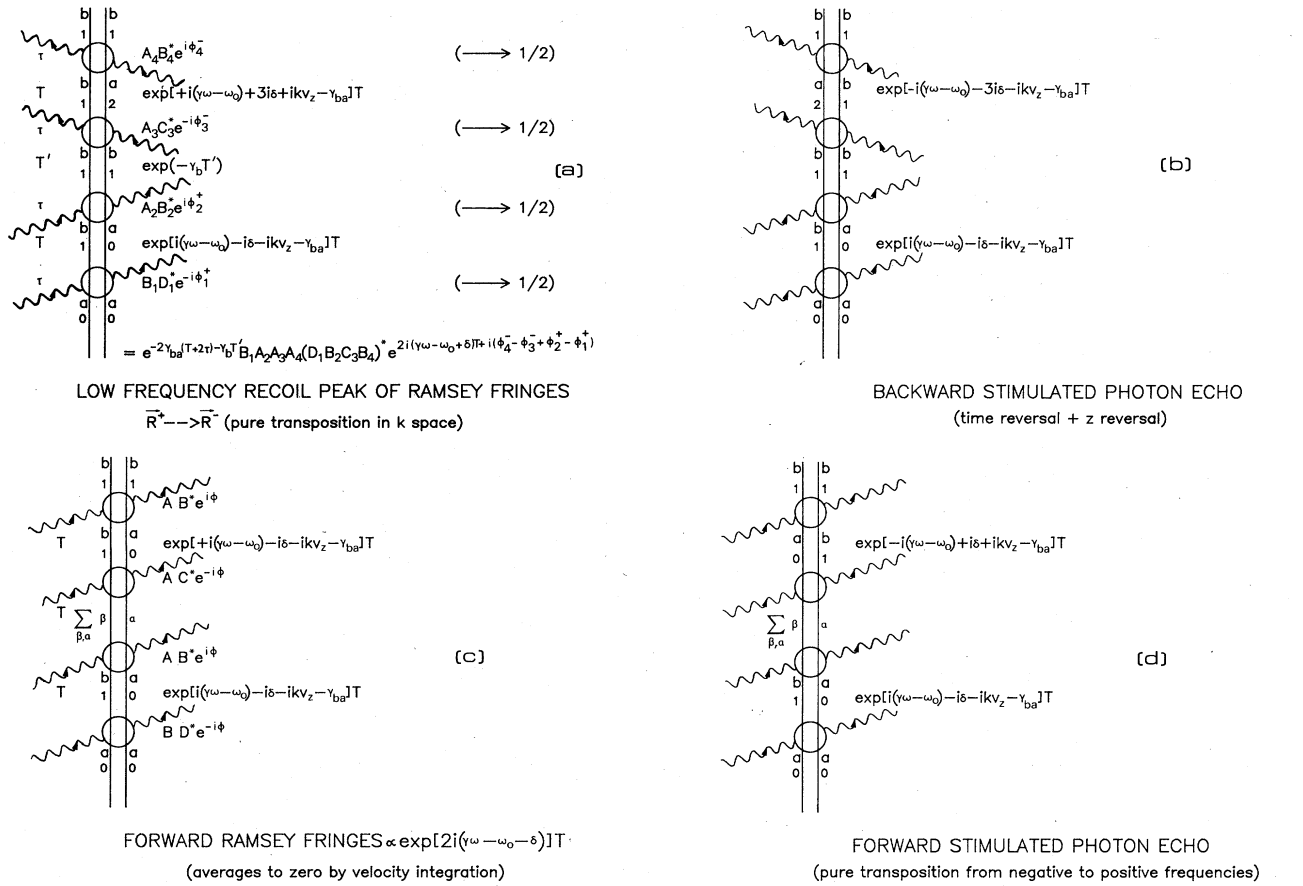

FIG. 5. (a) Strong-field density-matrix diagram for the low-frequency recoil component of Ramsey fringes. The product of the factors appearing at each vertex and of the three propagators which gives the contribution of the diagrams is explicitly written on the figure. One should add the complex conjugate term corresponding to the complex conjugate diagram. A similar diagram where $\langle 1|\tilde{\rho}_{bb}|1\rangle$ is replaced by $\langle 0|\tilde{\rho}_{aa}|0\rangle$ yields the contribution of the high-frequency recoil component. These two processes correspond to a pure transposition in k space reversing only the sign of the Doppler phase. (b) One of the diagrams corresponding to the backward stimulated photon echo. In this case the combination of both time and space (z) reversals (equivalently transpositions in both ω and k spaces) results in no change of the Doppler dephasing and the process averages to zero by velocity integration (but would exist for a nonreversing inhomogeneous dephasing mechanism[25]). (c) This process ("forward Ramsey fringes") is considered, in contrast with those of (a), as an example where the Doppler phase does not reverse and which will therefore average to zero by velocity integration. (d) Strong-field density-matrix diagram corresponding to the familiar forward stimulated photon echo (pure transposition from negative to positive frequencies equivalent to a time reversal). The two central zones can either be two successive $\pi/2$ pulses or coalesce into a single π pulse.

for

$$\langle m|\tilde{\rho}_{\alpha\alpha}|m'\rangle=\tilde{\alpha}_m\tilde{\alpha}^*_{m'}\,.$$

In the case of traveling waves the following transformation matrix is used at each vertex:

$$\begin{bmatrix} A & Be^{-i\varphi} \\ Ce^{i\varphi} & D \end{bmatrix} \otimes \begin{bmatrix} A^* & B^*e^{i\varphi} \\ C^*e^{-i\varphi} & D^* \end{bmatrix}. \tag{26}$$

We give in Fig. 5 some examples illustrating the usefulness of these diagrams for our purpose. A simple inspection of the total Doppler phase tells whether the process averages to zero or not by velocity integration. By looking at the frequency dependence one can easily recognize oscillating terms (fringes) or usual photon echo terms (with time reversal)[24] and obtain their recoil shift.

We see on the diagrams that for the usual stimulated photon echo the phase information carried by ρ_{ba} in the first half is transferred to ρ_{ab} in the second half. Since these two quantities vary with opposite frequencies this is a transposition of the information from the $\exp(i\omega t)$ domain to the $\exp(-i\omega t)$ domain and vice versa, which is equivalent to a time reversal.[25] Furthermore, if R_1 is multiplied by a coefficient α, R_2 being antisymmetric with respect to the interchange of ρ_{ab} and ρ_{ba} is multiplied by $-\alpha$. We recover the usual picture of the photon echo in which a symmetry is performed with respect to the $\hat{1},\hat{3}$ plane.[24]

For Ramsey fringes the phase information carried by ρ_{ba} in the first dark zone is transferred back to ρ_{ba} after interaction with the two central zones but, this time, with a transposition from the e^{ikz} domain to the e^{-ikz} domain

which is equivalent to a space (z) reversal. This is sufficient to reverse the Doppler dephasing (it is important to note that in contrast to the usual photon echo it is the dephasing mechanism which is reversed). Since there is no interchange of the indices b and a, $\vec{R}^-$ is collinear to $\vec{R}^+$.

If either none (forward Ramsey fringes) or both (stimulated backward photon echo) of these transpositions take place the Doppler phase subsists and the corresponding terms average to zero by velocity integration. Note that for any inhomogeneous dephasing mechanism, which does not reverse by z reversal, only the photon echo contributions subsist after integration over the distribution of frequencies.

VII. COMPARISON WITH STANDING WAVES

In the case of standing waves the transformation matrix for the vector

$$\begin{pmatrix} \vdots \\ \tilde{a}_m \\ \tilde{b}_{m-1} \\ \vdots \end{pmatrix}$$

can be deduced from the 2×2 matrix for

$$\begin{pmatrix} \sum \tilde{b}_m e^{imk(z+v_z t)} \\ \sum \tilde{a}_m e^{imk(z+v_z t)} \end{pmatrix}$$

derived in Ref. 21, with the assumption $\Omega_3=0$ in each field zone (see also Ref. 20)

$$\begin{pmatrix} \cos\frac{\Theta}{2} & i\sin\frac{\Theta}{2} \\ i\sin\frac{\Theta}{2} & \cos\frac{\Theta}{2} \end{pmatrix}, \tag{27}$$

where

$$\Theta = 4\Omega_{ba}\cos(kz+kv_z t_1+\varphi)\tilde{U}(kv_z)\,, \tag{28}$$

$$\tilde{U}(kv_z) = \int_{-\infty}^{+\infty} \cos kv_z\tau\, U(v_x\tau)\,d\tau\,. \tag{29}$$

For this purpose we use the following expansions:

$$\cos\frac{\Theta}{2} = J_0[2\Omega_{ba}\tilde{U}(kv_z)] + 2\sum_1^\infty (-1)^j J_{2j}[2\Omega_{ba}\tilde{U}(kv_z)] \times \cos 2j(kz+kv_z t_1+\varphi)\,, \tag{30}$$

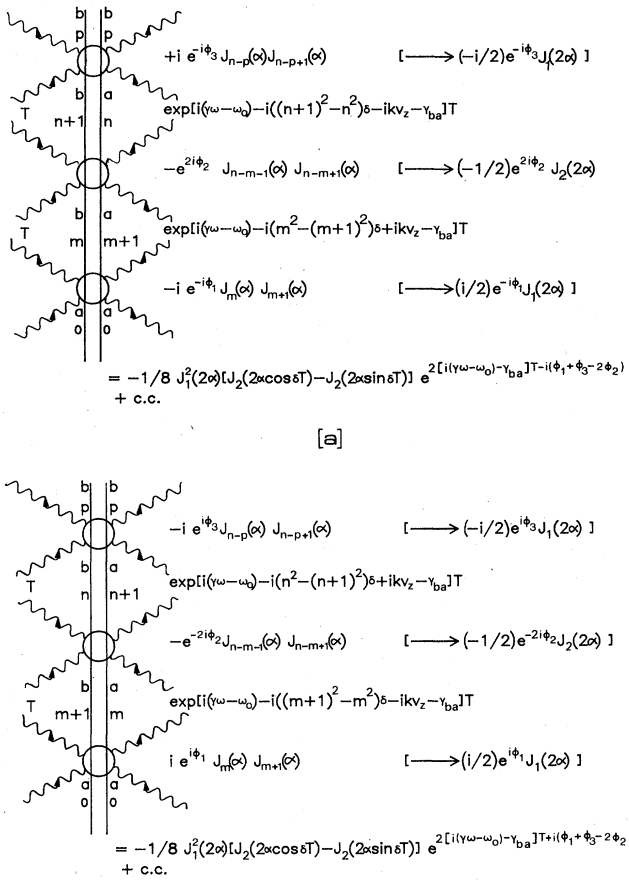

FIG. 6. Strong-field density-matrix diagrams for Ramsey fringes in the case of three standing waves. Only the contributions coming from the first spatial harmonic of the off-diagonal density-matrix elements freely precessing in the dark zones have been represented (similar diagrams can be drawn for higher harmonic contributions). The overall contribution of each type of diagram has been obtained by summation over the integer numbers m,n,p and is given in the figure with $\alpha=2\Omega_{ba}\tilde{U}(kv_z)$. When the recoil is neglected the factor corresponding to each vertex is obtained directly from (35) and is given between brackets for comparison with the traveling-wave case [Fig. 5(a)].

$$\sin\frac{\Theta}{2} = 2\sum_{j=0}^{\infty}(-1)^j J_{2j+1}[2\Omega_{ba}\tilde{U}(kv_z)] \times \cos[(2j+1)(kz+kv_z t_1+\varphi)]\,. \tag{31}$$

Hence the transformation between the incoming and outcoming vectors

$$\begin{pmatrix} \vdots \\ \tilde{a}_{m+2} \\ \tilde{b}_{m+1} \\ \tilde{a}_m \\ \tilde{b}_{m-1} \\ \vdots \end{pmatrix}_{t_1^+} = \begin{pmatrix} \cdots & J_0 & i(-1)^0 J_1 e^{i\varphi} & (-1)^1 J_2 e^{2i\varphi} & i(-1)^1 J_3 e^{3i\varphi} & \cdots \\ \cdots & i(-1)^0 J_1 e^{-i\varphi} & J_0 & iJ_1 e^{i\varphi} & -J_2 e^{2i\varphi} & \cdots \\ \cdots & -J_2 e^{-2i\varphi} & +iJ_1 e^{-i\varphi} & J_0 & iJ_1 e^{i\varphi} & \cdots \\ \cdots & -iJ_3 e^{-3i\varphi} & -J_2 e^{-2i\varphi} & iJ_1 e^{-i\varphi} & J_0 & \cdots \end{pmatrix} \begin{pmatrix} \vdots \\ \tilde{a}_{m+2} \\ \tilde{b}_{m+1} \\ \tilde{a}_m \\ \tilde{b}_{m-1} \\ \vdots \end{pmatrix}_{t_1^-}, \tag{32}$$

i.e., the generic element of the matrix is

$$A_{m+p,m}=i^p J_p e^{ip\varphi} . \tag{33}$$

The same strong-field density-matrix diagrams can be used as in the traveling-wave case with, this time, the proper Bessel functions at each vertex. As an example the diagrams of Fig. 6 correspond to Ramsey fringes with three standing waves (lowest harmonic order contributions to ρ_{ba} in the dark zones) where we have used the following sum rules:

$$\sum_{m \text{ even}} J_m(\alpha)J_{m+r}(\alpha)e^{i(2m+r)\delta}=\tfrac{1}{2}[i^r J_r(2\alpha\sin\delta)+J_r(2\alpha\cos\delta)] ,$$

$$\sum_{m \text{ odd}} J_m(\alpha)J_{m+r}(\alpha)e^{i(2m+r)\delta}=\tfrac{1}{2}[i^r J_r(2\alpha\sin\delta)-J_r(2\alpha\cos\delta)] .$$

If one is not interested by the recoil shift but only by the integer $m_\alpha-m_\beta$ indicating which harmonic of the density matrix is considered, it is possible to avoid complicated resummation of Bessel functions by starting with the direct product of two matrices

$$\begin{bmatrix} \cos\frac{\Theta}{2} & i\sin\frac{\Theta}{2} \\ i\sin\frac{\Theta}{2} & \cos\frac{\Theta}{2} \end{bmatrix} \otimes \begin{bmatrix} \cos\frac{\Theta}{2} & -i\sin\frac{\Theta}{2} \\ -i\sin\frac{\Theta}{2} & \cos\frac{\Theta}{2} \end{bmatrix} = \frac{1}{2} \begin{bmatrix} 1+\cos\Theta & -i\sin\Theta & i\sin\Theta & 1-\cos\Theta \\ -i\sin\Theta & 1+\cos\Theta & 1-\cos\Theta & i\sin\Theta \\ i\sin\Theta & 1-\cos\Theta & 1+\cos\Theta & -i\sin\Theta \\ 1-\cos\Theta & i\sin\Theta & -i\sin\Theta & 1+\cos\Theta \end{bmatrix} \tag{34}$$

and then only use the expansions (31) in Bessel functions with a double argument.

The transformation table which connects Fourier components of

$$\begin{bmatrix} \tilde{b} \\ \tilde{a} \end{bmatrix} \otimes \begin{bmatrix} \tilde{b}^* \\ \tilde{a}^* \end{bmatrix}$$

differing by $2j$ or $2j+1$ in their harmonic order is readily obtained from (34)

$$\frac{e^{2ij\varphi}}{2} \begin{bmatrix} \delta_{j0}+(-1)^j J_{2j} & -i(-1)^j J_{2j+1}e^{i\varphi} & i(-1)^j J_{2j+1}e^{i\varphi} & \delta_{j0}-(-1)^j J_{2j} \\ -i(-1)^j J_{2j+1}e^{i\varphi} & \delta_{j0}+(-1)^j J_{2j} & \delta_{j0}-(-1)^j J_{2j} & i(-1)^j J_{2j+1}e^{i\varphi} \\ i(-1)^j J_{2j+1}e^{i\varphi} & \delta_{j0}-(-1)^j J_{2j} & \delta_{j0}+(-1)^j J_{2j} & -i(-1)^j J_{2j+1}e^{i\varphi} \\ \delta_{j0}-(-1)^j J_{2j} & i(-1)^j J_{2j+1}e^{i\varphi} & -i(-1)^j J_{2j+1}e^{i\varphi} & \delta_{j0}+(-1)^j J_{2j} \end{bmatrix} . \tag{35}$$

This table provides a generalization, for arbitrary laser profiles, of the usual formulas of the gas laser theory with plane waves.[26–28]

We have indicated in front of each of the vertices of Fig. 6 the relevant matrix element from (35). By straightforward multiplication of all the factors appearing on the diagrams we recover the expression giving the contribution of each of them.[21] Thanks to these diagrams we can make a direct quantitative comparison of Ramsey fringes in various geometries. If we compare the diagrams corresponding to traveling waves to those corresponding to standing waves with the assumption of ideal excitation conditions:

$$A_1=A_2=A_3=A_4=D_1=D_2=D_3=D_4=\frac{1}{\sqrt{2}} ,$$

$$B_1=B_2=B_3=B_4=C_1=C_2=C_3=C_4=\frac{i}{\sqrt{2}}$$

($\pi/2$ pulses for $v_z=0$) we see that, adding the two recoil contributions, the two differ by a factor J_1 in the first and last vertices and by a factor J_2 in the combined action of the two middle vertices. If we add the mirror image contributions in the case of the standing wave we end up with a factor $2\,J_1^2\,J_2$ which gives a signal at the most $\simeq\frac{1}{3}$ of the traveling waves signal (the contributions from higher harmonics is negligible in these conditions). This factor explains well the difference in contrast that we observe between the two geometries and is also confirmed by experiments on Ca led in parallel with ours at the PTB in Braunschweig to test this theory.[29]

As a third case let us consider a diagram in which the first and third interaction vertices are with oppositely traveling waves and the middle interaction is with a standing wave (geometry proposed by Shimoda[14]). It is clear from Fig. 7(a) that we lose a factor $J_2\sim 0.5$ with respect to the purely traveling-wave case.

A final advantage of the traveling-waves case is that the recoil splitting contraction is absent[11,19] and furthermore the central dark space can be used to let the upper state decay get rid of the low-frequency recoil peak.[21]

Finally we may easily consider more complicated interaction sequences. Figure 7(b) corresponds to the standing-wave-induced backward photon echo introduced in Ref. 30. It is a combination of the usual forward echo with the Ramsey fringe scheme of Fig. 7(a), with time reversal in the second dark zone and z reversal in the third one. This process has therefore a detuning sensitivity which the usual echo does not have.

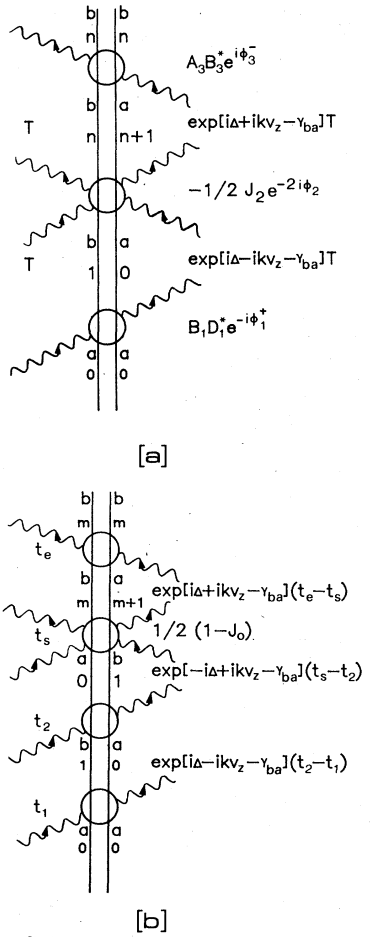

FIG. 7. Strong-field density-matrix diagrams corresponding to successive interactions with a combination of traveling and standing waves. (a) Ramsey fringes interaction geometry of Ref. 14. (b) Standing-wave-induced backward photon echo of Ref. 30.

VIII. CONCLUSION

As a conclusion, (1) we have demonstrated a new interaction geometry for high-resolution spectroscopy both experimentally and theoretically. This new method should be very useful for optical frequency standards, e.g., with Ca (Ref. 29) or I_2 in the visible. The potentiality for much higher resolution is illustrated by a preliminary experiment, where a 4.5 cm distance between Gaussian beams was used, resulting in a fringe pattern of period 10.42 kHz displayed on Fig. 8 (see also Ref. 31). (2) We have given graphical representations of processes involving spatially separated fields which allowed a comparison of Ramsey fringes with stimulated photon echoes as well as a comparison between various interaction geometries.

Thanks to these representations we have reached a clear quantitative understanding of the improvement in contrast provided by the traveling-waves interaction geometry for optical Ramsey fringes.

Note added. The term "photon echo" could be generalized to any mechanism in which a rephasing process of the polarization takes place and gives rise to a reemitted field (this polarization may also interact with an applied field whenever there is such a field). Within this generalization of the photon echo concept, Ramsey fringes would then be considered also as a backward stimulated photon echo. But in the present paper, we have reserved the term photon echo strictly to processes in which the pseudospin has a very-well-defined trajectory which is a symmetry about the $\hat{1}$-$\hat{3}$ plane and more simply a π rotation about the $\hat{1}$ axis (field axis) in the case of $\pi/2$ pulses. This is equivalent to a pure transposition $\rho_{ab}\rightarrow\rho_{ba}$ from the negative frequency domain to the positive frequency domain and vice versa or to a time reversal as explained in Sec. VI. This definition corresponds to the description of photon echoes found now in most textbooks [see, for example, M. Sargent, M. O. Scully, and W. E. Lamb, Laser Physics (Addison-Wesley, Reading, Mass., 1974) p. 218]. With this restricted definition of a photon echo the rephasing mechanism of the polarization that takes place in the Ramsey fringes process is indeed different from what happens in the usual photon echo as illustrated by the pseudospin trajectory of Fig. 3: after the two central-field zones $\vec{R}_{\text{ret}}^{-}$ is collinear to the direction that $\vec{R}^{+}$ had before them (whereas the usual definition of photon echoes corresponds to $\vec{R}_{\text{adv}}^{-}$ which is indeed obtained from $\vec{R}^{+}$ by a π rotation about the field axis). The contribution of $\vec{R}_{\text{adv}}^{-}$ averages to zero by velocity integration in Doppler broadened media. For these media, $\vec{R}_{\text{ret}}^{-}$ is therefore the only part of the pseudospin which rephases itself together and leads to what would be called a photon echo in a generalized definition but is here called simply the Ramsey fringes signal. On the contrary, for other media (for which there is no sign reversal of the dephasing process with the laser beam direction of propagation) it is $\vec{R}_{\text{adv}}^{-}$ which rephases itself and gives rise to a *true* backward stimulated photon echo (with our definition of this process). Independently from the names given to the two processes it is essential to make a clear distinction between the respective contributions of $\vec{R}_{\text{adv}}^{-}$ and $\vec{R}_{\text{ret}}^{-}$ which are completely different for the two types of media since it is one or the other which gives rise to the rephased polarization radiating in the backward direction or which interacts with the last field.

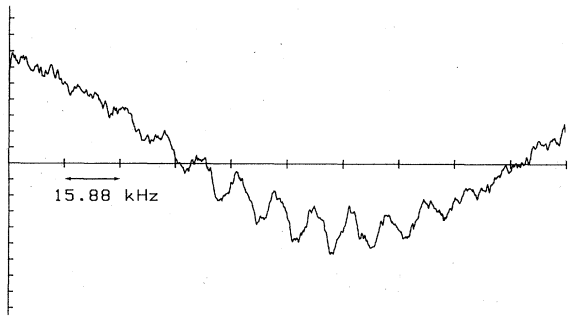

FIG. 8. High-resolution Ramsey fringes (FWHM: 5 kHz) obtained with traveling waves separated by 4.5 cm. The time constant is 0.1 s and 25 sweeps of duration 51 s have been added.

Noted added in proof. In Fig. 5(a) the factors $AB^*e^{i\phi}$ and $AC^*e^{-i\phi}$ appearing at the second and third vertices correspond only to the specific diagram for which $\alpha=\beta=b$.

ACKNOWLEDGMENTS

The authors are indebted to Ch. Chardonnet and to Ch. Tanguy for their critical reading of the manuscript and helpful comments. This work was supported in part by DRET (Direction des Recherches Etudes et Techniques) and by North Atlantic Treaty Organization (NATO).

[1]Ch. J. Bordé, Ph.D. thesis, University of Paris VI, 1972.
[2]N. F. Ramsey, Phys. Rev. **78**, 695 (1950).
[3]Y. V. Baklanov, B. Y. Dubetski, and V. P. Chebotayev, Appl. Phys. **9**, 171 (1976).
[4]Y. V. Baklanov, V. P. Chebotayev, and B. Y. Dubetski, Appl. Phys. **11**, 201 (1976).
[5]J. C. Bergquist, Ph.D. thesis, University of Colorado, 1978.
[6]J. C. Bergquist, S. A. Lee, and J. L. Hall, Phys. Rev. Lett. **38**, 159 (1977).
[7]R. L. Barger, J. C. Bergquist, T. C. English, and D. J. Glaze, Appl. Phys. Lett. **34**, 850 (1979).
[8]R. L. Barger, Opt. Lett. **6**, 145 (1981).
[9]Ch. Salomon, Ch. Bréant, Ch. J. Bordé, and R. L. Barger, J. Phys. (Paris) Colloq. **42**, C8-3 (1981), and references therein.
[10]Ch. J. Bordé, C. R. Acad. Sci. Ser. B **284**, 101 (1977).
[11]Ch. J. Bordé, in *Laser Spectroscopy III* (Springer, Berlin, 1977).
[12]T. E. Gough, R. E. Miller, and G. Scoles, Appl. Phys. Lett. **30**, 338 (1977).
[13]T. W. Mossberg, R. Kachru, S. R. Hartmann, and A. M. Flusberg, Phys. Rev. A **20**, 1976 (1979); T. W. Mossberg and S. R. Hartmann, *ibid.* **23**, 1271 (1981).
[14]N. Hata and K. Shimoda, Appl. Phys. **22**, 1 (1980); M. Baba and K. Shimoda, Appl. Phys. **24**, 11 (1981).
[15]S. Avrillier, J.-M. Raimond, Ch. J. Bordé, D. Bassi, and G. Scoles, Opt. Commun. **39**, 311 (1981).
[16]A. Boschetti (private communication).
[17]Ch. J. Bordé, S. Avrillier, A. Van Lerberghe, Ch. Salomon, Ch. Bréant, D. Bassi, and G. Scoles, Appl. Phys. B **28**, 82 (1982).
[18]Ch. Salomon, Ch. Bréant, A. Van Lerberghe, G. Camy, and Ch. J. Bordé, Appl. Phys. B **29**, 153 (1982).
[19]Ch. J. Bordé, in *Advances in Laser Spectroscopy,* North Atlantic Treaty Organization ASI Series (Plenum, New York, 1983).
[20]Ch. J. Bordé, S. Avrillier, A. Van Lerberghe, Ch. Salomon, D. Bassi, and G. Scoles, J. Phys. (Paris) Colloq. **42**, C8-15 (1981).
[21]Ch. J. Bordé, Rev. Cethedec-Ondes et Signal **NS83—1**, 1 (1983).
[22]W. T. Payne, Am. J. Phys. **20**, 253 (1952).
[23]R. P. Feynman, F. L. Vernon, and R. W. Hellwarth, J. Appl. Phys. **28**, 49 (1957).
[24]See, for example, M. Sargent, M. O. Scully, and W. E. Lamb, *Laser Physics* (Addison-Wesley, Reading, Mass., 1974).
[25]Ch. J. Bordé, in *Quantum Optics and Gravitation,* North Atlantic Treaty Organization ASI Series (Plenum, New York, 1983), and references therein, especially, N. S. Shiren, Appl. Phys. Lett. **33**, 299 (1978); A. Yariv and J. Auyeung, IEEE J. Quantum Electron. **QE—15**, 224 (1979).
[26]B. J. Feldman and M. S. Feld, Phys. Rev. A **1**, 1375 (1970).
[27]K. Uehara and K. Shimoda, Jpn. J. Appl. Phys. **10**, 623 (1971).
[28]J.-L. Le Gouet and P. R. Berman, Phys. Rev. A **20**, 1105 (1979).
[29]J. Helmcke, D. Zevgolis, and B. U. Yen. Appl. Phys. B **28**, 83 (1982).
[30]N. W. Carlson, A. G. Yodh, and T. W. Mossberg, Phys. Rev. Lett. **51**, 35 (1983).
[31]Ch. Salomon, S. Avrillier, A. Van Lerberghe, and Ch. J. Bordé, in *Laser Spectroscopy VI* (Springer, Berlin, 1983).